2

TGAL-85-3

FINITE DIFFERENCE CRATERING SUPPORT
Task 1 FINAL REPORT
Magnitude Determination of Cratering and
Non-Cratering Nuclear Explosions

Final Technical Report
for Task 1 submitted to

DARPA/DSO/GSD
1400 Wilson Blvd.
Arlington, Va. 22209

contract; MDA903-84-C-0289
Department of the Army
Defense Supply Service - Washington
Room 1D 245, The Pentagon
Washington, D. C. 20310

submitted by
K.L. McLaughlin, I.N. Gupta, and R. Wagner
Teledyne Geotech Alexandria Labs
314 Montgomery
Alexandria, Va. 22314

May 1985

The views and conclusions contained in this document are those of the authors and should not be interpreted as representing the official policies, either expressed or implied, of the Defense Advanced Research Projects Agency or the U.S. Government.

TGAL-85-3

FINITE DIFFERENCE CRATERING SUPPORT
Task 1 FINAL REPORT
Magnitude Determination of Cratering and Non-Cratering Nuclear Explosions

Final Technical Report
for Task 1 submitted to

DARPA/DSO/GSD
1400 Wilson Blvd.
Arlington, Va. 22209

contract; MDA903-84-C-0289
Department of the Army
Defense Supply Service - Washington
Room 1D 245, The Pentagon
Washington, D. C. 20310

APPROVED FOR PUBLIC RELEASE; DISTRIBUTION UNLIMITED.

submitted by
K.L. McLaughlin, I.N. Gupta, and R. Wagner
Teledyne Geotech Alexandria Labs
314 Montgomery
Alexandria, Va. 22314

May 1985

use " quotes throughout

ABSTRACT

The ratio of the "a" phase and "max" phase of presumed Shagan River contained and cratering explosions are studied across the WWSSN network of short period stations. The amplitude of the "a" phase of the presumed cratering explosion of Jan~~uary~~ 15, 1965 is found to be systematically larger in comparison to the "max" amplitude of this cratering explosion when compared to contained explosions in the vicinity of the cratering explosion, (i.e.) ~~In other words~~ the log of the ratio of the amplitudes of the "a" and "max" phase, log(Pmax/Pa), is on average smaller for the Jan~~uary~~ 9 15, 1965 cratering explosion than for any of the contained explosions studied. Several methods were used to study the systematics of the log(Pmax/Pa) value across the WWSSN network. The preferred method for determining ~~determination of~~ the average log(Pmax/Pa) was a maximum-likelihood method that includes the effects of data truncation of clipping for Pmax and non-detection of Pa. Assuming that the "a" phase amplitude of the cratering explosion is unaffected by the influence of the non-linear free surface interaction, the corrected magnitude for the cratering explosion is 0.17 to 0.27 magnitude units larger than its 5.88 WWSSN network magnitude. If the cratering explosion is credited with a yield of 125 KT then a 125 KT contained explosion in the Shagan River test site should produce a WWSSN network m_b between 6.05 to 6.15. Assuming a log(yield) slope of 1.0 the analysis predicts a 150 KT explosion should produce a WWSSN network m_b between 6.13 and 6.23. The analysis assumes that the Pa phase amplitude is the same for cratering and contained explosions of the same yield, and the WWSSN network at distances between 20 and 90 degrees.

INTRODUCTION

A detailed determination of cratering and non-cratering short period P-wave magnitudes was conducted, in order to better understand the short period magnitude biases between different test sites. The P-wave mb's were determined using the initial "a" phase, the "b" phase and the maximum P-wave amplitudes in the first 5 seconds. Magnitudes based on amplitude, A, and amplitude corrected for period, A/T, were considered. The differential between these different methods of P-wave amplitude determination was studied as a network average and on a station-by-station average. It has been suggested that the initial displacement of the teleseismic P wave is not as affected by the free surface effects that are manifested in the pP arrival. The detonation of a shallow explosion results in a non-linear "reflection" of energy at the free surface that must appear near the time of the linear-elastic pP wave. The scaling of this pP with depth and yield remains a major problem in the understanding of the teleseismic short-period waveforms. The P+pP waveform is certainly observed for deep explosions while shallow explosions show less definitive evidence of the P+pP waveform. It is argued that the "a" phase is less affected by the free surface reflection even for cratering explosions where there is no true reflection of energy at the free surface. This argument implies that the "a" phase will scale more linearly with yield than the "b" and maximum phases commonly used in magnitude determination. The depth correction for the "a" phase is therefore unnecessary, while it may be considered necessary for "b" and "max" phases.

Given that the Pmax/Pa amplitude ratio can be determined for the "normally" buried and cratering explosion created teleseismic P waves, a check on the yield of the East Kazakh explosions can be formulated from the difference between the

log(Pmax/Pa) for the scale-depth explosion and the cratering (125 KT) explosion at East Kazakh. A bias for the cratering explosion as measured using the log(Pmax/T) or log(Pmax) as a measure of magnitude can be determined. We can define this predicted "bias" as Ξ, where

$$\Xi = log\,(Pmax\,/\,Pa\,)_{scale-depth} - log\,(Pmax\,/\,Pa\,)_{crater}$$

The mb magnitude of a scale-depth explosion of the same yield as the cratering explosion of Jan. 15, 1965 would then be

$$mb_{125KT} = mb_{crater} + \Xi .$$

Teleseismic P waves were synthesized for the Von-Seggern Blandford (1972) source time function observed through a WWSSN short period instrument. The pP-P delay time, τ in seconds, was assumed to scale by either τ_1=0.07 $W^{1/3}$ or τ_2=0.12 $W^{1/3}$ (τ in seconds, W in KT). Attenuation parameterized by t^* values of 0.20 and 0.45 seconds was introduced into the synthetic waveforms. The pP was assumed to be a "linear" reflection with decreasing amplitude with increasing frequency as in Blandford et al. (1984). The synthetics were also computed for no pP contribution. These "linear" models predict log(Pc/Pa) values greater than the values for no pP as listed below.

t^* (sec)	τ (sec)	$log\,(Pc\,/\,Pa\,)_{scale-depth} - log\,(Pc\,/\,Pa\,)_{no-pP}$
0.45	0.37	0.22
0.45	0.64	0.19
0.20	0.37	0.24
0.20	0.64	0.14

Depending upon the choice of t^* and the scale-depth, the estimated value of Ξ varies between 0.14 and 0.24. The same calculations were conducted for the LRSM short period instrument which has a broader bandwidth than the WWSSN short period instrument with virtually the same results. We would expect that pP-P times may vary

over a test site if the testing practices or geology are not uniform. We would expect that the effective t^* would vary over a network of stations.

In order to predict the Ξ for 150 KT events at 200 meters (cratering) and 500 meters (scale depth), while beginning to take into account the non-linear effects, we examine the suite of granite calculations made by Bache et al. (1980). For a set of depths ranging from 150 meters to 1000 meters, they predict teleseismic waveforms for a 150 KT event observed with a KS-36000 seismometer and a t^* = 0.8 sec. The following predicted differences between mb(Pc) and mb(Pa) for these calculated depths are taken from Figure 15 and Table 5 of Bache et al. (1980).

h (meters)	mb(Pc)-mb(Pa)
159.4	0.49
207.2	0.50
253.0	0.50
398.5	0.57
531.3	0.62
797.0	0.69
1000.0	0.63

The difference between the shallow source, about 200 meters, and the deep source, about 500 meters, is Ξ = 0.12 magnitude units. Consequently, given the assumptions in the Bache et al. (1980) model we would predict that the "a" phase of the cratering explosion is relatively larger, compared to the "c" phase by about 0.12 magnitude units for a similarly sized explosion near scale-depth. This is slightly less than predicted by the "linear" model presented above.

Several factors may conspire to obscure the predicted log(Pmax/Pa) distribution for a real network recording real explosions. These factors include the variance of amplitude data due to focussing-defocussing, the variance of attenuation due to source-receiver paths, and the generation of P coda due to scattering. P coda may be such that the

"Pmax" in the first 5 seconds of the P wave is not the "c" phase as in the case of synthetic P waveforms in a horizontally layered earth. The following section attempts to determine if the log(Pmax/Pa) is "stable" for East Kazakh events as a function of magnitude and locations in the proximity of the cratering event of Jan. 15, 1965. Following the determination of the stability of log(Pmax/Pa), the value of Ξ is estimated for events with mb $\approx$ 5.9 and epicenters near the January 15, 1965 cratering event.

DATA ANALYSIS OF TELESEISMIC P WAVES

The Jan 15, 1965 cratering explosion in East Kazakh had an announced yield of 125 kilotons (Nordyke, 1973). The explosion crater (and the lake it became) is clearly visible on LANDSAT images. The event has been used by several researchers to relocate East Kazakh events and calibrate teleseismic networks for the computation of travel times from the East Kazakh test site (Rodean, 1979; Shore, 1982). Several events of similar yield have occurred within several kilometers of the crater. We have used the WWSSN network to determine the average station differentials between mb(b), mb(max), and mb(a) for a number of East Kazakh events. Several of these events are in close proximity to the location and yield of the Jan 15, 1965 cratering explosion. The ISC origins of the E. Kazakh events studied in this report are listed in Table I.

Table I. ISC ORIGINS

Event	Origin Time	N. Lat.	E. Long.	mb	δ (km)
15jan65	05:59:58.4	49.88	78.96	5.8	0.0
19jun68	05:05:57.4	49.96	79.05	5.4	11.0
11sep69	04:01:57.5	49.77	78.03	5.0	68.1
30nov69	03:32:57.3	49.94	78.98	6.0	6.8
14dec73	07:46:57.1	50.03	79.02	5.8	17.2
27apr75	05:36:57.2	49.94	79.02	5.6	8.0
04jul76	02:56:57.5	49.85	78.97	5.8	3.4
07dec76	04:56:57.5	49.87	78.89	5.9	5.2
11jun78	02:56:57.7	49.88	78.81	5.7	10.8
15sep78	02:36:57.3	49.91	78.94	6.0	3.6

The δ is the distance, km, from each ISC epicenter to the ISC cratering epicenter. The relative locations are probably only good to within a few km or so.

Five methods were used to estimate the log(Pmax/Pa) average for each event and combinations of events. In the first method, the maximum likelihood (ML) network magnitude was calculated for each event using log(A) and log(A/T) for the "a", "b",

and "max" phase of the P wave at each station. The amplitude, A, was corrected for the gain of the WWSSN station at the estimated period, T. The network magnitudes suffer from the requirement for station corrections. In the second method, the log(Pmax/Pa) value was averaged over the network for each event. This method suffers from non-detections, clippings, and non-uniform station distributions. In the third method, only common stations were used for two pairs of events. This method suffers from the fact that due to station down-time, non-detections and clipping, the subset of stations common to two events is always less than the number of stations available for each event. The fourth method, was a maximum likelihood estimate of the log(Pmax/Pa) over the network for each event. The fifth method, was a maximum likelihood estimate of the log(Pmax/Pa) value for combinations of events. The fourth and fifth methods combine to give the least biased estimates of the value of log(Pmax/Pa) since the clipping of Pmax and non-detections of Pa may be accounted for by the maximum likelihood procedure. Furthermore, the ML log(Pmax/Pa) values are not affected by station corrections since the station correction is canceled by the ratio of Pmax/Pa.

Network magnitudes were determined to estimate the network magnitude differentials between mb(a), mb(b), and mb(max). The method of maximum likelihood magnitude determination (Ringdal 1976) was used to account for both clipping and non-detections across the network. For network magnitude determination, the Veith and Clawson (1972) tables were applied with individual station corrections from Blandford et al. (1984). These station corrections are listed in Table IIa. Additional tests were made using residuals derived from a recent study by Ringdal using ISC reported magnitudes tabulated in Table IIb. A plot of the Blandford et al. (1984) versus Ringdal residuals is shown in Figure 1. The correlation coefficient between the two sets of residuals is 0.61. Because the two sets of "station corrections" were derived in different ways and from

different data sets we chose to primarily use the Blandford et al. (1984) corrections because they were derived from an explosion data set with an effort to avoid bias between test sites. Furthermore the Blandford et al. (1984) station residuals constitute a more complete set of WWSSN stations. Figures 2 and 3 show the Ringdal (1984) station corrections versus North (1977) and the North (1977) versus Blandford et al. (1984) with correlations of 0.87 and 0.46 respectively..

Note that the Ringdal station residuals have standard errors of a single observation near 0.36 magnitude units. This is a good estimate of the "typical" width of the distribution of magnitudes from a network of stations. Therefore, in order to see expected biases between a cratering and non-cratering event near 0.1 magnitude units with σ_{mean} = 0.05 requires on the order of 40 or more stations in a network.

For each event and at each station, the maximum P-wave amplitude in the first 5 seconds was measured, along with the "b" phase, and the "a" phase. In the absence of a measurable phase, the clipping, or noise level was measured. This procedure applied to "max", "b", and "a" phase alike. In general, teleseismic distances between 20 and 95 degrees were used, however, experiments using only stations 30 and 90 degrees from the epicenter, rarely changed the network magnitude by more than 0.05 magnitude units. These distance ranges are common for teleseismic mb-yield determinations. Furthermore, log(A/T) for the Pmax phase is used almost universally to determine mb. Consequently the most important bias, Ξ, that can be determined is for Pmax using log(A/T). Calculations were performed for log(A) magnitude as well.

The network maximum-likelihood magnitude results are shown in Table IIIa, IIIb, and IIIc. The magnitudes were calculated using both the log(A) and log(A/T) from the station amplitude and period readings.

Table IIIa. Maximum-Likelihood Magnitudes
20 < Δ < 95
Station Effects From Table IIa.

Event	mb(a)	mb(a)	mb(b)	mb(b)	mb(max)	mb(max)
	A	A/T	A	A/T	A	A/T
15jan65	5.44	5.50	5.67	5.73	5.82	5.88
19jun68	4.58	4.64	5.02	5.07	5.23	5.30
11sep69	3.76	3.84	4.15	4.22	4.52	4.57
30nov69	5.37	5.42	5.74	5.78	5.94	5.98
14dec73	5.22	5.24	5.52	5.55	5.75	5.78
27apr75	4.89	4.98	5.22	5.31	5.44	5.53
04jul76	5.21	5.26	5.59	5.64	5.91	5.96
07dec76	4.89	4.94	5.39	5.44	5.57	5.62
11jun78	5.23	5.30	5.55	5.60	5.84	5.90
15sep78	5.35	5.42	5.65	5.72	5.84	5.90

Table IIIb. Maximum-Likelihood Magnitudes
30 < Δ < 90
Station Effects From Table IIa.

Event	mb(a)	mb(a)	mb(b)	mb(b)	mb(max)	mb(max)
	A	A/T	A	A/T	A	A/T
15jan65	5.43	5.50	5.66	5.72	5.80	5.87
19jun68	4.56	4.64	5.03	5.08	5.23	5.28
11sep69	3.71	3.84	4.15	4.21	4.49	4.52
30nov69	5.36	5.41	5.72	5.77	5.90	5.94
14dec73	5.16	5.18	5.46	5.49	5.70	5.72
27apr75	4.76	4.86	5.13	5.23	5.27	5.37
04jul76	5.15	5.19	5.54	5.58	5.86	5.90
07dec76	4.85	4.91	5.27	5.33	5.44	5.49
11jun78	5.13	5.18	5.45	5.50	5.73	5.78
15sep78	5.35	5.42	5.62	5.69	5.78	5.85

Table IIIc. Maximum-Likelihood Magnitudes
$30 < \Delta < 90$
Station Effects From Table IIb.

Event	mb(a)	mb(a)	mb(b)	mb(b)	mb(max)	mb(max)
	A	A/T	A	A/T	A	A/T
15jan65	5.45	5.52	5.68	5.74	5.83	5.89
19jun68	4.58	4.62	5.05	5.09	5.24	5.30
11sep69	3.74	3.74	4.14	4.20	4.51	4.54
30nov69	5.41	5.47	5.76	5.81	5.97	6.02
14dec73	5.24	5.26	5.54	5.56	5.77	5.79
27apr75	4.83	4.94	5.20	5.31	5.36	5.45
04jul76	5.25	5.29	5.63	5.67	5.95	6.00
07dec76	4.97	5.03	5.39	5.45	5.54	5.59
11jun78	5.24	5.29	5.56	5.61	5.85	5.90
15sep78	5.44	5.51	5.71	5.78	5.87	5.94

The network magnitude differences for mb(Pmax)-mb(Pa), mb(Pb)-mb(Pa), and mb(Pmax)-mb(Pb) for both log(A) and log(A/T) are shown in Tables IVa, IVb, and IVc. These tables simply represent the differences that can be calculated from Tables IIIa, IIIb, and IIIc, respectively.

Table IVa. Maximum-Likelihood Differences From Table IIIa.
$20 < \Delta < 95$

Event	Pmax-Pa	Pmax-Pa	Pb-Pa	Pb-Pa	Pmax-Pb	Pmax-Pb
	(A)	(A/T)	(A)	(A/T)	(A)	(A/T)
19jun68	0.65	0.66	0.44	0.43	0.21	0.23
11sep69	0.76	0.73	0.39	0.38	0.37	0.35
30nov69	0.57	0.56	0.37	0.36	0.20	0.20
14dec73	0.53	0.54	0.30	0.31	0.23	0.23
27apr75	0.55	0.55	0.33	0.33	0.22	0.22
04jul76	0.70	0.70	0.38	0.38	0.32	0.32
07dec76	0.68	0.68	0.50	0.50	0.18	0.18
11jun78	0.61	0.60	0.32	0.30	0.29	0.30
15sep78	0.49	0.48	0.30	0.30	0.19	0.18
AVE	0.62(.08)	0.61(.08)	0.37(.06)	0.37(.06)	0.25(.06)	0.25(.06)
15jan65	0.38	0.38	0.23	0.23	0.15	0.15

Table IVb. Maximum-Likelihood Differences From Table IIIb.
30 < Δ < 90

Event	Pmax-Pa (A)	Pmax-Pa (A/T)	Pb-Pa (A)	Pb-Pa (A/T)	Pmax-Pb (A)	Pmax-Pb (A/T)
19jun68	0.67	0.64	0.47	0.44	0.20	0.20
11sep69	0.78	0.68	0.44	0.37	0.34	0.31
30nov69	0.37	0.37	0.36	0.36	0.18	0.17
14dec73	0.54	0.54	0.30	0.31	0.24	0.23
27apr75	0.51	0.51	0.37	0.37	0.14	0.14
04jul76	0.71	0.71	0.39	0.39	0.32	0.32
07dec76	0.59	0.58	0.42	0.42	0.17	0.16
11jun78	0.60	0.60	0.32	0.32	0.28	0.28
15sep78	0.43	0.43	0.27	0.27	0.16	0.16
AVE	0.58(.12)	0.56(.11)	0.37(.06)	0.36(.05)	0.23(.07)	0.22(.07)
15jan65	0.37	0.37	0.23	0.22	0.14	0.15

Table IVc Maximum Likelihood Magnitude Differences From Table IIIc.
30 < Δ < 90

Event	Pmax-Pa (A)	Pmax-Pa (A/T)	Pb-Pa (A)	Pb-Pa (A/T)	Pmax-Pb (A)	Pmax-Pb (A/T)
19jun68	0.66	0.68	0.47	0.47	0.19	0.21
11sep69	0.77	0.80	0.40	0.46	0.37	0.34
30nov69	0.56	0.55	0.35	0.34	0.21	0.21
14dec73	0.53	0.53	0.30	0.30	0.23	0.23
27apr75	0.53	0.51	0.37	0.37	0.16	0.14
04jul76	0.70	0.71	0.38	0.38	0.32	0.33
07dec76	0.57	0.56	0.42	0.42	0.15	0.14
11jun78	0.61	0.61	0.32	0.32	0.29	0.29
15sep78	0.43	0.43	0.27	0.27	0.16	0.16
AVE	0.60(.10)	0.60(.11)	0.36(.06)	0.37(.07)	0.23(.07)	0.23(.07)
15jan65	0.38	0.37	0.23	0.22	0.15	0.15

The standard deviation of the event magnitude difference population is shown in "()" for the population of non-cratering events. Although the cratering event difference, mb(Pmax)-mb(Pa), lies outside the one sigma range for all the columns in Table IV, there are several events for which the relative sizes of "Pa" and "Pmax" are closer to the cratering shot than the non-cratering average. From the point of view of similarity of size (mb) and proximity (δ from Table I.), if we take those events for which mb > 5.6

and δ < 10 km then the average estimated bias, Ξ, between the the cratering and non-cratering shot ranges between 0.10 and 0.32 based on mb(Pmax)-mb(Pa) and 0.07 and .27 based on the mb(Pb)-mb(Pa) values. These numbers vary depending upon the choice of log(A) or log(A/T) or the comparison of the "Pa" phase to the "Pb" phase or to the "Pmax" phase. Unquestionably, the "Pa" phase is, on the average, larger with respect to the "Pb" or "Pmax" phases for the cratering event than for the general population of E. Kazakh contained explosions. The cratering explosion has, on average, only a slightly smaller ratio of of Pmax/Pb.

In order to examine the relative sizes of the "Pa" vs "Pmax" on a station-by-station basis, and to avoid the unnecessary use of station corrections, the average station-by-station average of log(Pmax/Pa) was determined for each event over the stations detecting both "Pmax" and "Pa". The results are tabulated in the following Table.

Table V. Station Average mb(Pmax)-mb(Pa) With Sigma

Event	log(Pmax/Pa)	log(Pmax/Pa)
	log(A/A)	log[(A/T)/(A)]
Jun68	0.43(.04)	0.41(.04)
Sep69	0.34(.05)	NA
Nov69	0.52(.03)	0.51(.03)
Dec73	0.39(.04)	0.39(.05)
Apr75	0.51(.05)	0.53(.05)
Jul76	0.58(.04)	0.57(.04)
Dec76	0.56(.07)	0.57(.07)
Jun78	0.50(.04)	0.51(.04)
Sep78	0.42(.03)	NA
AVE	0.46(.02)	0.46(.02)
Jan65	0.38(.03)	0.39(.03)

The standard deviation of the mean is shown in "()". Again, we observe that the log(Pmax/Pa) is smaller for the cratering shot. The difference between the cratering shot

and the non-cratering explosion is $\Xi = 0.08(0.04)$. However if we limit the comparison to shots with mb > 5.6 and δ < 10 km then $\Xi \geqslant 0.12$ magnitude units for all but the Sep78 event. The difference in the log(Pmax/Pa) between the Sep78 and Jan65 events is only 0.04(0.03). The Sep78 event clearly stands out among the larger non-cratering events.

Since the networks may change in subtle ways from one event to another, we performed the same calculations, network and station-by-station, using only common stations. Only stations that were common to both the Jan65 and the Dec73 events or common to both the Jan65 and Sep78 events.

Table VI. Network Max-Like Magnitude Differences
$30 < \Delta < 95$
Common Stations only.

Event	mb(max)-mb(a) (A)&(A)	mb(max)-mb(a) (A/T)&(A)	# stn
Jan65	0.34	0.40	31
Dec73	0.50	0.46	31
Jan65	0.33	0.38	22
Sep78	0.42	0.51	22

Using common stations only for the Jan65-Dec73 and Jan65-Sep78 comparisons increases the differences between the log(Pmax/Pa) averaged over the entire network. The differences are then 0.16 and 0.09 for log(A) respectively. The Dec73 event is 17 km from the Jan65 event and may represent a different testing environment while the ISC location of the Sep78 event is within 10 km of the Jan65 event and it remains uncertain why the event has a different relative size of "Pa" versus "Pmax" than the general population of contained explosions.

Alternatively, one can calculate the station-by-station differences for a common set of stations.

Table VII. Station-by-Station Magnitude Differences
30 < Δ < 95
Common Stations Only

Event	log(Pmax/Pa)	log(Pmax/Pa)	# stn
	log(A/A)	log[(A/T)/(A)]	
Jan65	0.37(.04)	0.42(.04)	28
Dec73	0.46(.04)	0.50(.04)	28
Jan65	0.18(.03)	0.38(.05)	25
Sep78	0.42(.04)	0.53(.06)	25

The standard deviations of the mean are shown in "()". Using the data of Table VII, above, the differences between the Jan65 and Dec73 and Jan65 and Sep78 events for log(Pmax/Pa) are 0.09(.04) and 0.22(.04) respectively. The differences expressed in Tables VI and VII above are greater than expected given the quoted standard deviations of Table VII.

In order to eliminate the need for station corrections, and to account for the biasing effects of non-detection of Pa, and clipping of Pmax, the maximum-likelihood estimation technique was used to estimate the log(Pmax/Pa) over a network of stations. Several cases could be added to the case where measurement of Pmax and Pa could be made. This method has the advantage that there is a greater probability that the "Pa" phase may not be observed while the "Pmax" phase is observed. Consequently, if the correlation of "Pa" and "Pmax" amplitudes is not 100% then there will be preferential sampling of stations where the ratio (Pmax/Pa) is smaller than the norm. These cases are summarized in the following table.

Table VIII.			
	Pmax on scale	Pmax clipped	Pmax < noise
Pa on scale	signal	clipped	not used
Pa clipped	not used	not used	not used
Pa < noise	clipped	clipped	not used

Figures 4, 5 and 6 illustrate the use of the maximum likelihood approach to the estimation of the statistic log(Pmax/Pa). The arrows on the histograms represent the number of clipped values in the population of log(Pmax/Pa) measurements. The following results were found for the ten individual events.

Table IX. Maximum-Likelihood log(Pmax/Pa) Ratios

Event	log(Pmax/Pa)
19jun68	0.68(0.33)
11sep69	0.77(0.34)
30nov69	0.54(0.20)
14dec73	0.51(0.25)
27apr75	0.60(0.25)
04jul76	0.72(0.25)
07dec76	0.89(0.44)
11jun78	0.53(0.21)
15sep78	0.47(0.28)
AVE	0.63(0.13)
15jan65	0.41(0.24)

The "()" standard error given for each event is the maximum likelihood estimated population sigma for the log(Pmax/Pa) over the network. The standard error given for the "AVE" in the table is the standard error for the non-cratering explosion population. These results are in general agreement with the results from Tables V, VI, and VII. The average bias is estimated as, $\Xi = 0.63 - 0.41 = 0.22$, using all nine contained explosions. Figures 7, 8, and 9 compare the composite maximum likelihood fits to the combined populations of 7 non-cratering events 5 non-cratering events and 4 non-cratering events respectively. The 7 largest non-cratering events have a combined population of

log(Pmax/Pa) with an estimated mean of 0.58 (Figure 7) which implies $\Xi = 0.17$. The 5 non-cratering events (30 Nov 69, 14 Dec 73, 04 Jul 76, 07 Dec 76, and 15 Sep 78) have a combined population of log(Pmax/Pa) with an estimated mean of 0.60 (Figure 8) which implies $\Xi = 0.19$. The results for four events are shown in Figure 9 with an estimated mean of 0.68 and an implied $\Xi = 0.27$. The four non-cratering events chosen for Figure 9 are the same events used by Der et al. (1985) in for source deconvolution (Task 2, this contract) using the Shumway-Der multichannel deconvolution technique. These four events are 11jun78, 7jul76, 4jul76, and 27apr75. This analysis demonstrates the variability of the statistic log(Pmax/Pa) and implies that Ξ lies in the range between 0.17 and 0.27.

Of interest is that the typical population width, $\sigma_r = 0.29$, for log(Pmax/Pa) is only 20% less than the population width, $\sigma_0 = 0.36$, of station magnitude residuals. The average station residual σ from Table IIb is about 0.36 magnitude units. The individual station values of log(Pmax/Pa) contain a great deal of remaining scatter; although the amplitude of Pa is correlated to the amplitude of Pmax, the correlation is imperfect.

CONCLUSIONS

In conclusion, it appears that log(Pmax/Pa) is variable from shot to shot but that it generally is between 0.5 and 0.7 magnitude units. The P waveforms from the cratering event of Jan 15, 1965, on average, have values of log(Pmax/Pa) generally near to 0.4. The estimated bias to correct the mb(Pmax) for the cratering event to a contained shot with a yield of 125 Kt is then $\Xi = 0.10$ to .30 magnitude units. The preferred values depending upon the method used to estimate the difference $\Xi = \log(Pmax/Pa)_{scale-depth} - \log(Pmax/Pa)_{crater}$. The maximum likelihood estimates for the individual network values of log(Pmax/Pa) from Table IX are the most direct and least biased estimates of

the log(Pmax/Pa) values for each event. These estimates are the least biased by non-detection of Pa and clipping of Pmax. The estimates of Table IX are non influenced by the choice of station corrections, and they are not influenced by the choice of Veith and Clawson distance corrections.

The maximum likelihood estimates of log(Pmax/Pa) range from 0.58 to 0.68 depending upon the set of contained explosions that are chosen. The best estimate of the network mean of the log(Pmax/Pa) for the cratering explosion is 0.41. From these values, the estimated mb(Pmax) bias for the cratering explosion, Ξ, ranges from 0.17 to 0.27. From Table IIIa the mb(Pmax) for the cratering event is 5.88, and the implied unbiased mb(Pmax) estimate of the 15 Jan 65 cratering event is then 6.05 to 6.15. If we assume that the cratering explosion had a yield of 125 Kt, then a log(yield)-mb slope of 1.0 would give an estimate of 6.13 to 6.23 for the 150 Kt scale-depth shot. Given the uncertainties in the magnitude determinations and the uncertainties in the scaling laws for P+pP interference the conclusions are consistent with the estimated mb(150 Kt) value of 6.17 given by Blandford et al. (1984). It should be emphasized that such a prediction is based on the WWSSN network using distances between 20 and 90 degrees, the yield value of 125 Kt for the 15 Jan 65 cratering explosion, and the assumption that the Pa phase amplitude is the same for the cratering event and a contained explosion of the same yield.

However, events can be found within the East Kazakh test site with anomalous log(Pmax/Pa) values on the average over a network of teleseismic stations. The event of 15 Sep 78 had a network average value of log(Pmax/Pa) that was only 0.06 (from Table IX) larger than the cratering event. This investigation raises the question as to what mechanism could be responsible for the reduction in the Pmax of this event (or alterna-

tively larger Pa). Perhaps other information is available that indicates whether the 15 Sep 78 event was unusual. A cursory investigation of the WWSSN waveforms the the East Kazakh events studied did not reveal a marked difference between the waveforms of the 15 Sep 78 and other events. Furthermore, it is not always clear whether the cratering event is different from the remaining population of events until statistical averaging is performed on the log(Pmax/Pa) statistics; such is the stochastic nature of short period waveforms.

North and Fitch (1981) analyzed the surface waves of the 15 Sep 78 and 11 June 78 events as well as several others. They found the 15 Sep 78 event to be of "TYPE I"; the Rayleigh waves were not reversed at any observed azimuth. According to the North and Fitch (1981) epicenter relocations, the 11 June 78 and the 15 Sep 78 events are closer to each other than each is to the cratering event epicenter (see Figure 10 taken from North and Fitch, 1981). The 11 June 78 event appears to have a normal log(Pmax/Pa) distribution over the network.

Herrin and Goforth (1982) analyzed the Rayleigh waves of the 15 sep 78 event and although they did not observe reversed Rayleigh waves for the 15 Sep 78 explosion, they observed larger arrivals proceeding the main fundamental at KAAO and an apparent delay of the Rayleigh wave by 3 to 4 seconds at SHIO. How this applies to the log(Pmax/Pa) statistics is uncertain, for it is not clear how the Pmax amplitude would be relatively smaller for an event with tectonic complications.

Table IIa. Station Residuals for Network mb From Blandford et al. (1984)

aae	-0.34	aam	0.24	ade	0.22	afi	-0.10
aku	-0.10	alq	-0.25	anp	-0.56	ant	0.05
aqu	-0.24	are	0.11	atl	0.14	atu	-0.12
bag	-0.09	bdf	-0.01	bec	-0.12	bhp	-0.05
bks	0.14	bla	0.18	bog	-0.02	boz	0.07
bul	0.08	car	0.08	chg	-0.23	cmc	-0.31
col	0.21	cop	0.02	cor	0.27	cta	0.01
dag	0.00	dal	0.30	dav	-0.14	dug	0.05
eil	0.01	esk	-0.03	flo	0.39	fvm	0.19
gdh	-0.07	geo	-0.17	gie	-0.24	gol	-0.17
grm	-0.24	gsc	-0.02	gua	0.13	hkc	-0.23
hlw	-0.11	hn-	0.21	hnr	0.22	ist	0.08
jct	0.10	jer	-0.07	kbl	-0.02	kbs	-0.01
kev	-0.07	kip	0.20	kod	0.12	kon	0.13
krk	-0.27	ktg	-0.18	lah	0.25	lem	-0.29
lon	-0.09	lor	0.13	lpa	0.05	lpb	-0.13
lps	-0.14	lub	0.39	mal	-0.05	man	0.59
mat	-0.01	mds	0.27	mhi	0.05	mnn	0.24
msh	-0.10	mso	0.04	mun	-0.01	nai	0.06
nat	0.14	ndi	0.11	nha	0.05	nil	-0.20
nna	-0.02	nor	-0.59	np-	0.09	nur	0.03
ogd	0.00	oxf	0.59	pda	0.02	pel	-0.14
pmg	-0.15	poo	-0.03	pre	0.06	pto	-0.09
que	-0.28	qui	-0.03	rab	0.22	rar	-0.39
rcd	0.51	riv	-0.02	rk-	0.33	sba	-0.39
scp	0.06	sdb	0.04	seo	-0.06	sha	0.30
shi	-0.07	shk	-0.08	shl	0.02	sjg	-0.06
sna	0.29	sng	-0.12	som	0.50	spa	0.06
stu	-0.02	tab	0.01	tau	-0.28	tol	0.01
tri	-0.28	trn	-0.01	tuc	-0.06	ume	0.02
unm	-0.25	val	-0.09	wel	0.03	wes	-0.15
win	-0.22	ale	-0.04	asp	-0.05	bha	-0.28
bmo	-0.29	bng	-0.07	bns	0.20	can	-0.02
cir	-0.27	cll	0.20	clk	-0.27	cpo	-0.07
edm	0.37	eka	0.00	eur	-0.24	fur	0.10
gil	-0.04	grf	0.24	hfs	0.05	hyb	0.19
khc	0.10	kjf	0.09	kjn	0.14	kra	0.22
krr	-0.24	lao	-0.10	lju	0.29	mbc	0.14
mox	0.02	na0	-0.09	new	0.05	nie	-0.02
pmr	-0.08	pnt	0.13	pru	0.04	res	0.13
tfo	-0.32	tsk	-0.07	tul	0.21	ubo	-0.11
wmo	-0.17						

Table IIb. Ringdal Station Residuals

sta	B	σ	sta	B	σ	sta	B	σ
ADK	0.22	0.42	GRR	0.04	0.26	NAO	-0.10	0.33
ALE	-0.10	0.30	GUA	0.43	0.40	NDI	0.30	0.38
ALQ	-0.20	0.33	HFS	0.13	0.35	NEW	-0.07	0.39
ARE	0.17	0.32	HYB	0.26	0.32	NUR	0.11	0.46
ASP	0.09	0.39	ILT	0.08	0.32	NVL	0.23	0.35
BAG	0.26	0.32	IMA	-0.16	0.36	OBN	0.39	0.33
BDF	0.11	0.35	INK	0.25	0.29	PET	0.24	0.36
BDW	-0.15	0.35	IPM	0.10	0.36	PMG	0.27	0.38
BHA	-0.25	0.32	IRK	-0.03	0.31	PMR	-0.11	0.39
BJI	0.06	0.34	JAY	0.15	0.41	PNS	0.11	0.50
BKR	0.38	0.33	KBL	0.15	0.30	POO	0.19	0.35
BLC	0.21	0.29	KBS	0.12	0.32	PPI	0.08	0.41
BMO	-0.28	0.35	KEV	0.05	0.31	PRE	-0.08	0.40
BNG	0.01	0.41	KHC	0.03	0.26	PSI	-0.02	0.38
BOD	-0.02	0.34	KHE	0.37	0.31	QUE	0.21	0.46
BUL	-0.05	0.29	KHO	0.59	0.35	RAB	0.37	0.43
CAN	0.11	0.31	KIR	0.61	0.25	RES	0.04	0.33
CAR	0.14	0.40	KJF	0.16	0.28	SCH	0.27	0.34
CHG	-0.06	0.36	KOD	0.18	0.35	SES	0.42	0.28
CIR	-0.24	0.30	KRA	0.32	0.29	SHL	0.22	0.33
CLK	-0.24	0.29	KRP	0.43	0.36	SJG	0.19	0.35
CLL	0.16	0.26	KTG	-0.07	0.29	SPA	0.16	0.37
COL	0.07	0.34	LAO	0.04	0.35	STK	0.27	0.38
CPO	-0.02	0.35	LEM	0.11	0.39	SVE	0.37	0.31
CTA	0.07	0.39	LOR	-0.08	0.33	TIK	0.03	0.37
DAG	0.08	0.32	LPB	0.18	0.35	TOO	0.13	0.35
DUG	-0.04	0.31	LPS	0.12	0.38	TPT	0.09	0.34
EDM	0.43	0.28	MAIO	-0.11	0.37	TUC	-0.17	0.32
EKA	0.	0.29	MAT	-0.01	0.38	TUL	0.21	0.34
ELT	0.15	0.34	MAW	0.04	0.31	TUP	-0.35	0.40
EUR	-0.36	0.47	MBC	0.09	0.35	TVO	0.19	0.29
FFC	0.09	0.30	MIR	0.22	0.33	UBO	-0.13	0.38
FRB	0.37	0.29	MNG	0.11	0.39	UPP	0.60	0.33
FRU	0.35	0.33	MOX	0.07	0.25	WRA	-0.20	0.44
FVM	0.25	0.43	MOY	0.12	0.29	YAK	0.43	0.34
GBA	-0.07	0.42	MSO	-0.06	0.44	YKC	0.08	0.34
GDH	-0.05	0.30	MTD	-0.12	0.30	YSS	0.20	0.41
GRF	0.25	0.28	MTN	-0.08	0.38	ZAK	-0.11	0.33

REFERENCES

Bache, T.C., T.G. Barker, N. Rimer, and J.T. Cherry (1980). The Contributions of Two-Dimensional Source Effects to the Far-Field Seismic Source Signatures of Underground Nuclear Explosions, SSS-R-80-4569.

Blandford, R.R., R.H. Shumway, R. Wagner, and K.L. McLaughlin (1984). Magnitude Yield For Nuclear Explosions At Several Test Sites with Allowance for Effects of Truncated Data, Amplitude Correlation Between Events within Test Sites, and Absorption, and pP. *TGAL-TR-83-6. Teledyne Geotech,* Alexandria, Va. 22314.

Der, Z.A., R.H. Shumway, A.C. Lees, and E. Smart (1985) Multichannel Deconvolution of P Waves at Seismic Arrays, *TGAL-85-4. Teledyne Geotech Report,* Alexandria, Va. 22314.

Nordyke, M. (1973). A Review of Soviet Data on the Peaceful Uses of Nuclear explosions, UCRL-51414.

North, R.G. (1977). Station magnitude bias -- its determination, causes, and effects, Mass. Inst. Tech., Lincoln Laboratory, Technical Note 1977-24, Lexington, Massachusetts.

North, R.G., and T.J. Fitch (1981). Surface Wave Generation by Underground Nuclear Explosions. Unpublished manuscript.

Ringdal, F. (1976). Maximum likelihood estimation of seismic magnitude, *Bull. Seism. Soc. Am., 66,* 789-802.

Ringdal, F. (1984). Norsar Semi-Annual Report.

Rodean, H.C. (1979). ISC events form 1964 to 1976 at and near the nuclear testing ground in eastern Kazakhstan, *UCRL-52856. Lawrence Livermore Laboratory,* Livermore, Ca. 94550.

Shore, M.J. (1982). Seismic travel-time anomalies from events in the western Soviet Union. *Bull. Seism. Soc. Am., 72,* 113-128.

Veith, K.F. and G.E. Clawson (1972). Magnitude from short period P-wave data. *Bull. Seism. Soc. Am., 62,* 435-452.

von Seggern, D.H. and R.R. Blandford (1972). Source time functions and spectra for underground nuclear explosions, *Geophys. J. Roy. astr. Soc.*, *31*, 83-97.

FIGURE CAPTIONS

FIGURE 1. Blandford at al. (1984) stations corrections versus Ringdal (1984) station corrections. Correlation coefficient of 0.65.

FIGURE 2. North (1977) station corrections versus Ringdal (1984) station corrections. Correlation coefficient of 0.87.

FIGURE 3. North (1977) station corrections versus Blandford et al. (1984) station corrections. Correlation coefficient of 0.46.

FIGURE 4. Histogram of the log(Pmax/Pa) measurements for the 30 Nov 69 event. Clipped values of the log(Pmax/Pa) are indicated by right pointing arrows. There are 20 signal measurements, and 10 clipped measurements. The maximum likelihood estimate of the Gaussian distribution is plotted with a mean of 0.54 and a $\sigma = 0.20$.

FIGURE 5. Histogram of the log(Pmax/Pa) measurements for the 14 Dec 73 event. Clipped values of the log(Pmax/Pa) are indicated by right pointing arrows. There are 27 signal measurements, and 23 clipped measurements. The maximum likelihood estimate of the Gaussian distribution is plotted with a mean of 0.51 and a $\sigma = 0.25$.

FIGURE 6. Histogram of the log(Pmax/Pa) measurements for the 15 Sep 78 event. Clipped values of the log(Pmax/Pa) are indicated by right pointing arrows. There are 21 signal measurements, and 10 clipped measurements. The maximum likelihood estimate of the Gaussian distribution is plotted with a mean of 0.47 and a $\sigma = 0.28$.

FIGURE 7. Composite histogram for the 7 largest non-cratering events. 106 signals and 69 clipped measurements. Maximum likelihood estimate of the Gaussian distribution has mean 0.58 and $\sigma = 0.29$. Distribution for the 15 Jan 65 cratering event is shown above with mean 0.41 and $\sigma = 0.24$.

FIGURE 8. Composite histogram for the 5 largest non-cratering events. 72 signals and 55 clipped measurements. Maximum likelihood estimate of the Gaussian distribution has mean 0.60 and $\sigma = 0.29$. Distribution for the 15 Jan 65 cratering event is shown above with mean 0.41 and $\sigma = 0.24$.

FIGURE 9. Composite histogram for 4 non-cratering events. 38 signals and 26 clipped measurements. Maximum likelihood estimate of the Gaussian distribution has mean 0.68 and $\sigma = 0.33$. Distribution for the 15 Jan 65 cratering event is shown above with mean 0.41 and $\sigma = 0.24$.

FIGURE 10. Event relocations of selected E. Kazakh explosions taken directly from North and Fitch (1981). Crosses indicate the relocation from ISC locations indicated by small circles. Events 6/11/78, 9/15/78, and 1/15/65 are labeled A, B, and C respectively.

STATION CORRECTIONS (WW) **FIGURE 1**

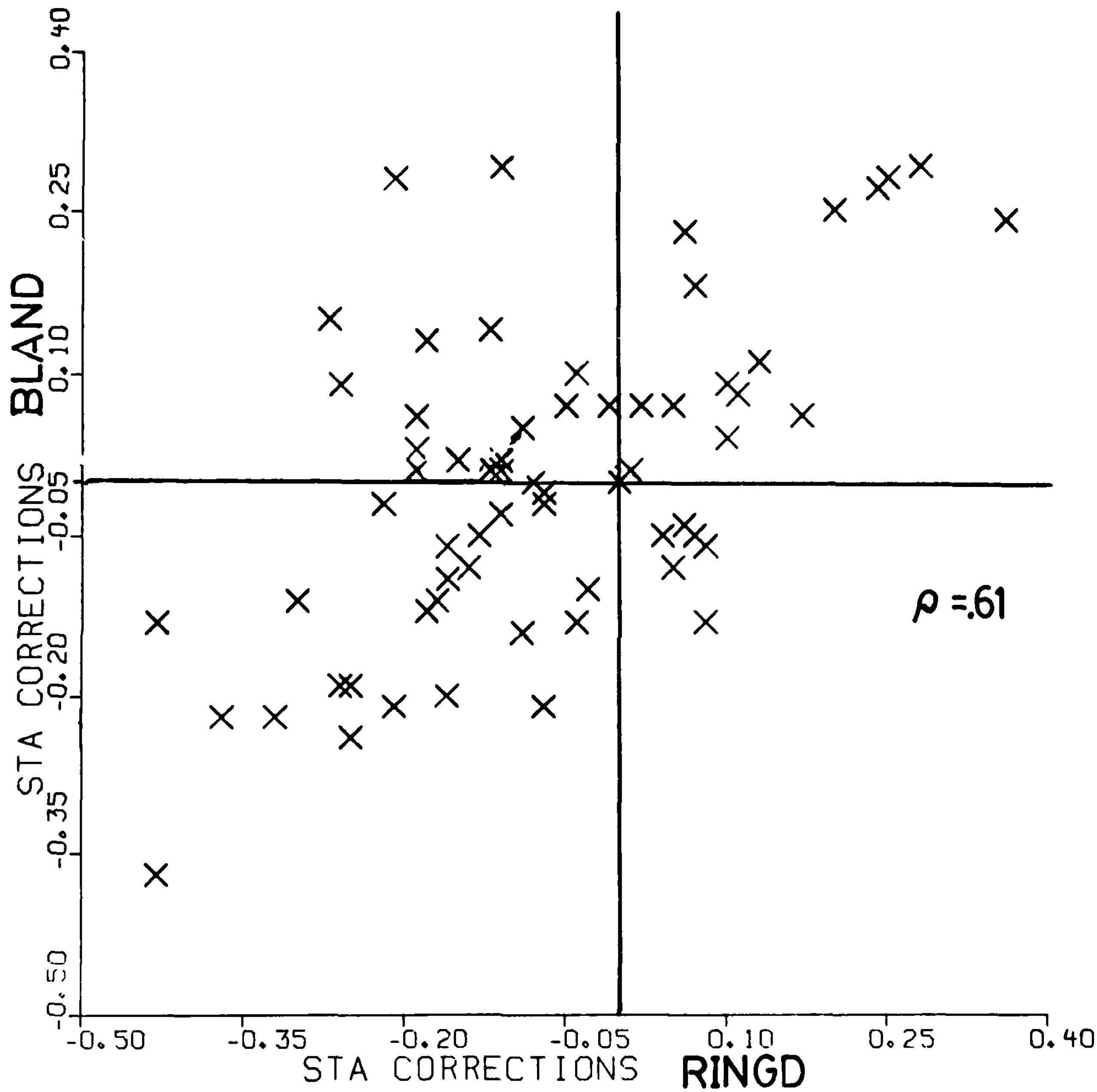

STATION CORRECTIONS (WW) **FIGURE 2**

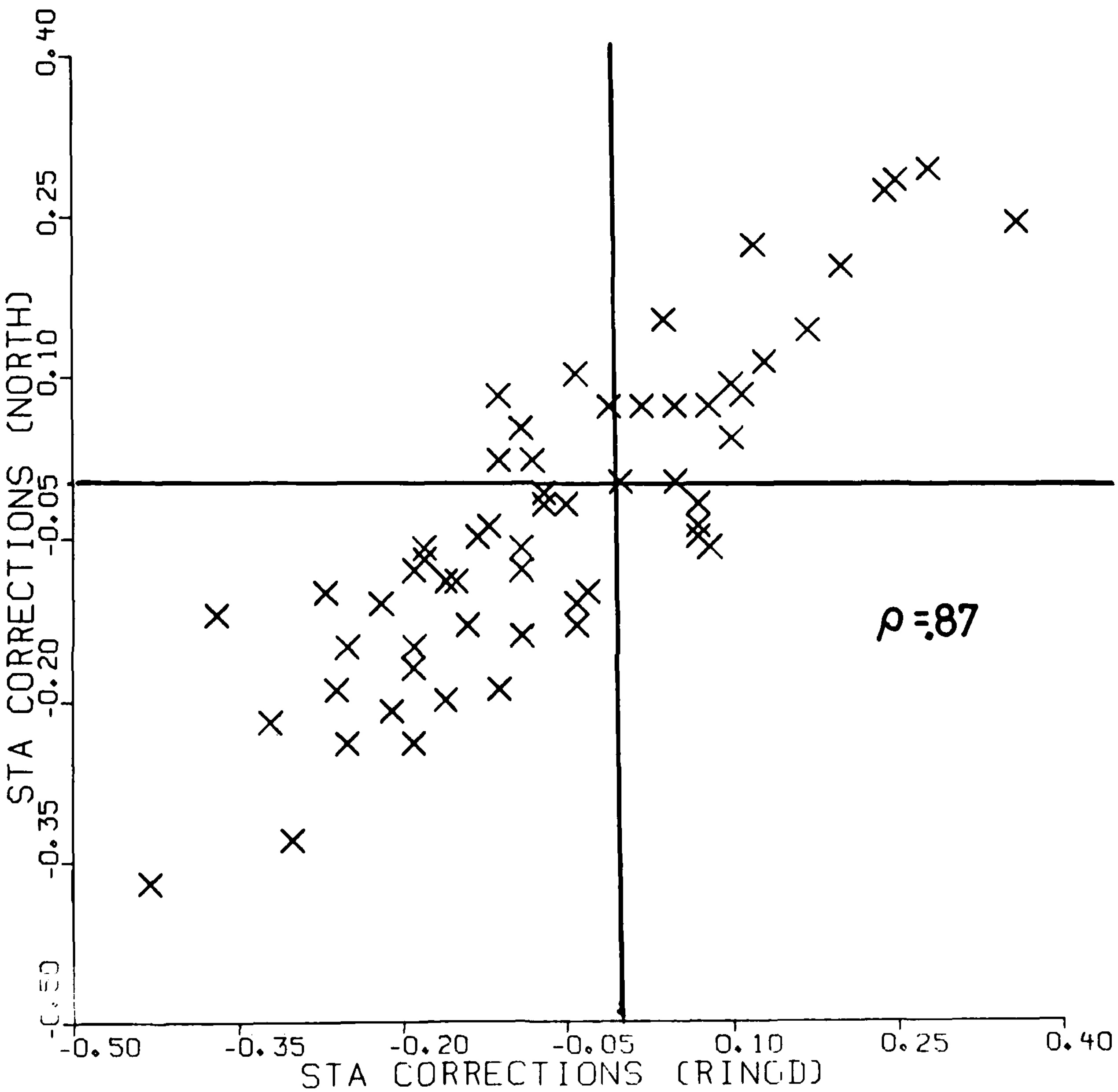

FIGURE 3

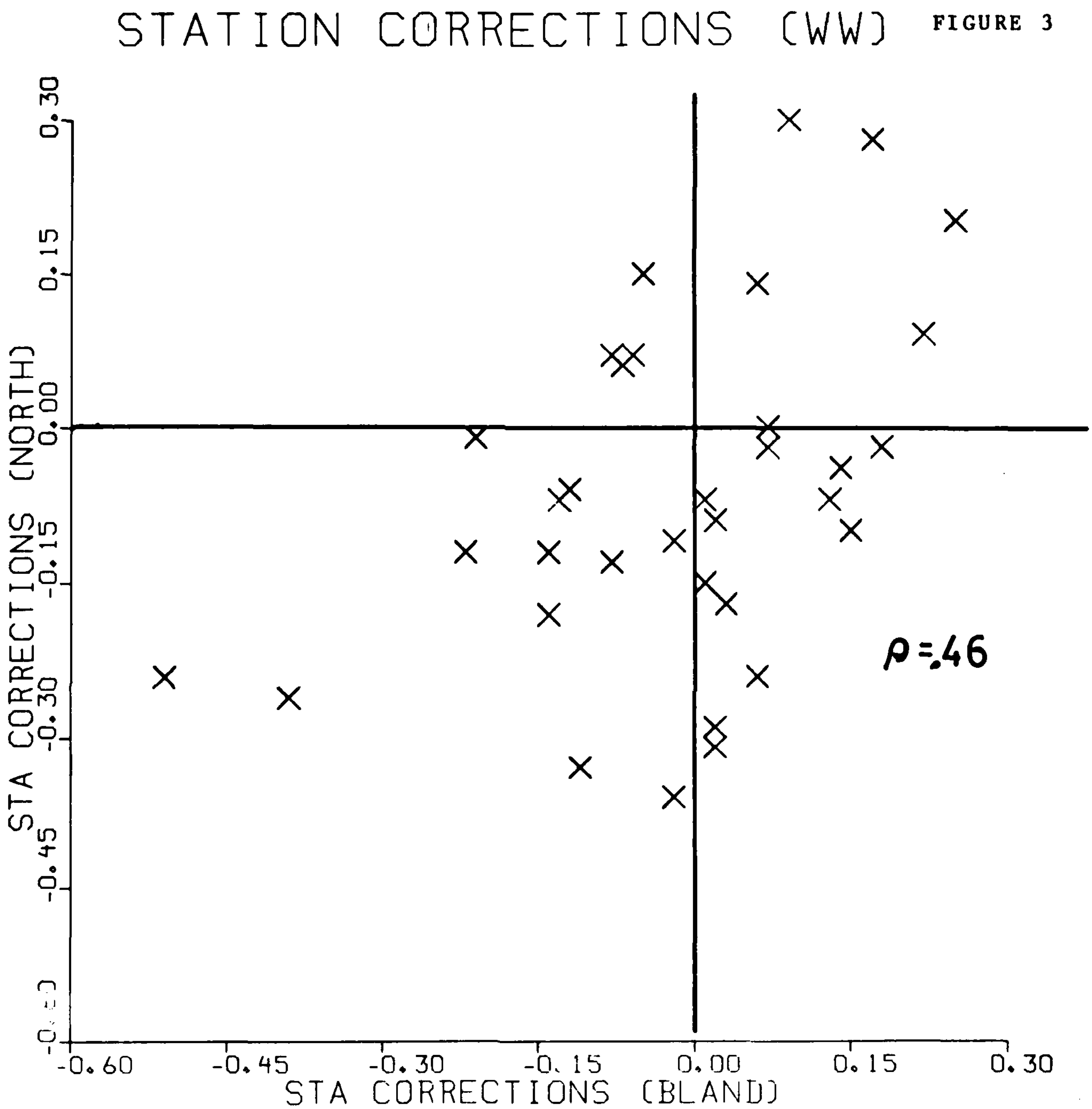
STATION CORRECTIONS (WW)
STA CORRECTIONS (NORTH)
0.30
0.15
0.00
-0.15
-0.30
-0.45
STA CORRECTIONS (BLAND)
-0.60
-0.45
-0.30
-0.15
0.00
0.15
0.30
ρ=.46

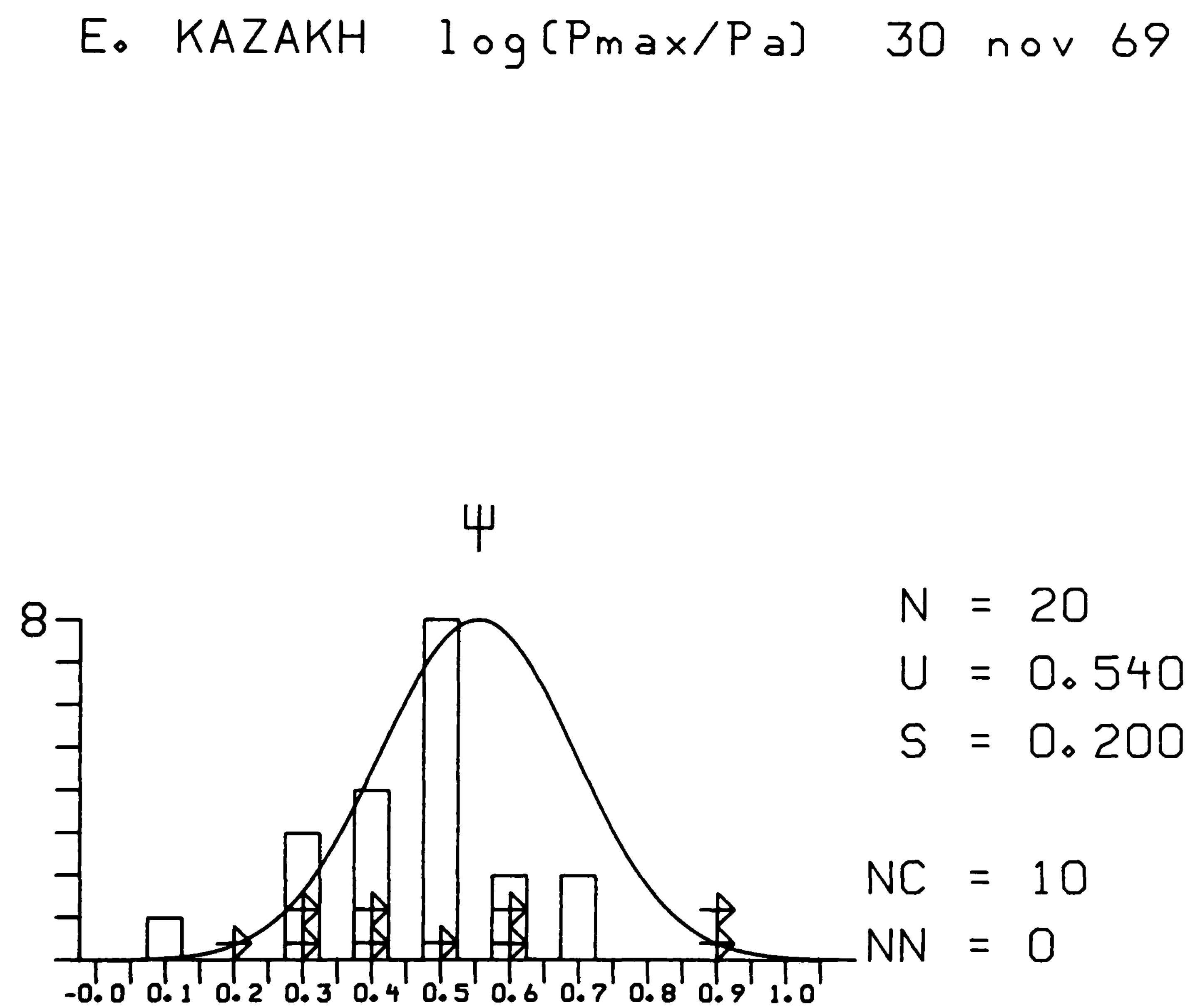
E. KAZAKH log(Pmax/Pa) 30 nov 69
Ψ
8
-0.0 0.1 0.2 0.3 0.4 0.5 0.6 0.7 0.8 0.9 1.0
N = 20
U = 0.540
S = 0.200
NC = 10
NN = 0

FIGURE 4

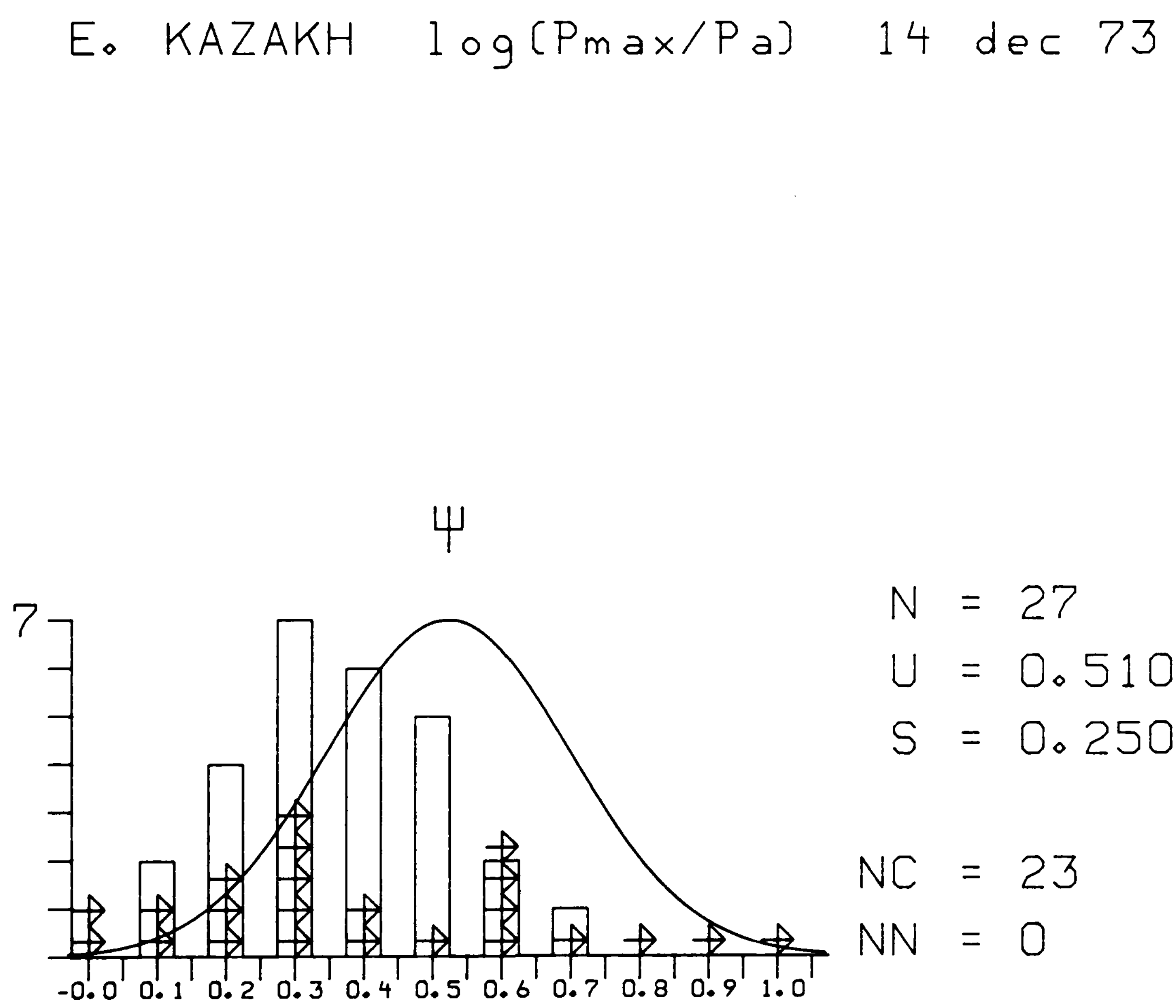
E. KAZAKH log(Pmax/Pa) 14 dec 73
ψ
7
-0.0
0.1
0.2
0.3
0.4
0.5
0.6
0.7
0.8
0.9
1.0
N = 27
U = 0.510
S = 0.250
NC = 23
NN = 0

FIGURE 5

E. KAZAKH log(Pmax/Pa) 15 sep 78

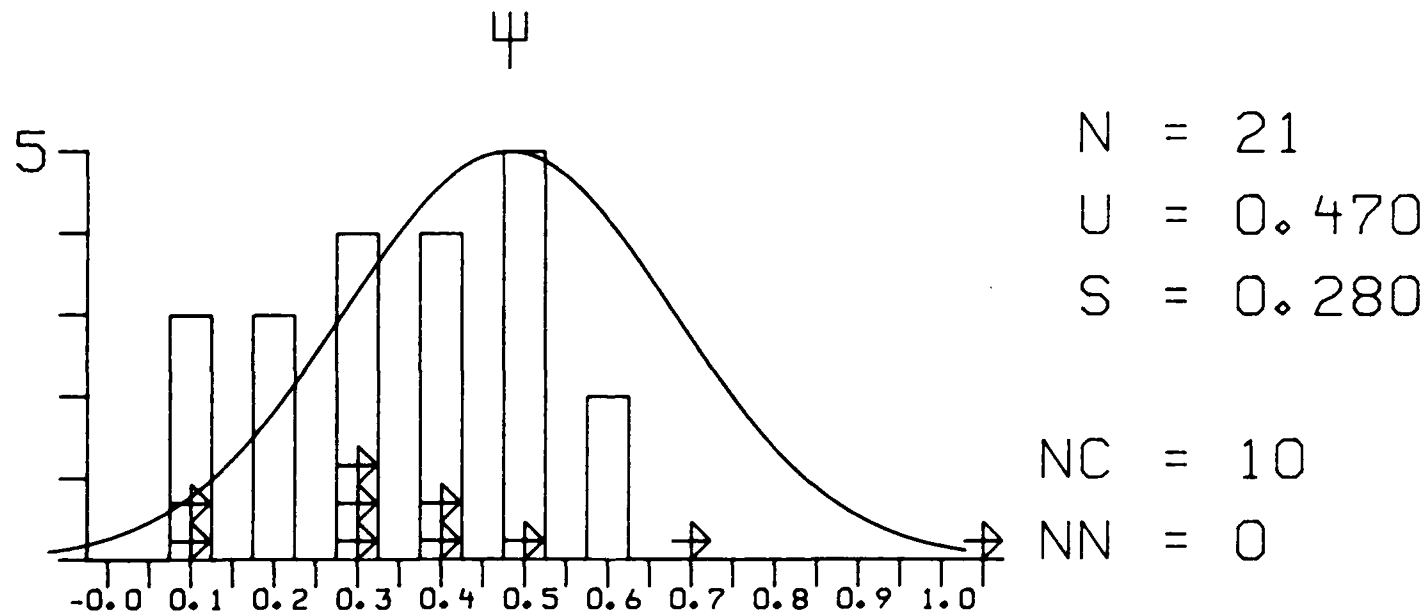

FIGURE 6

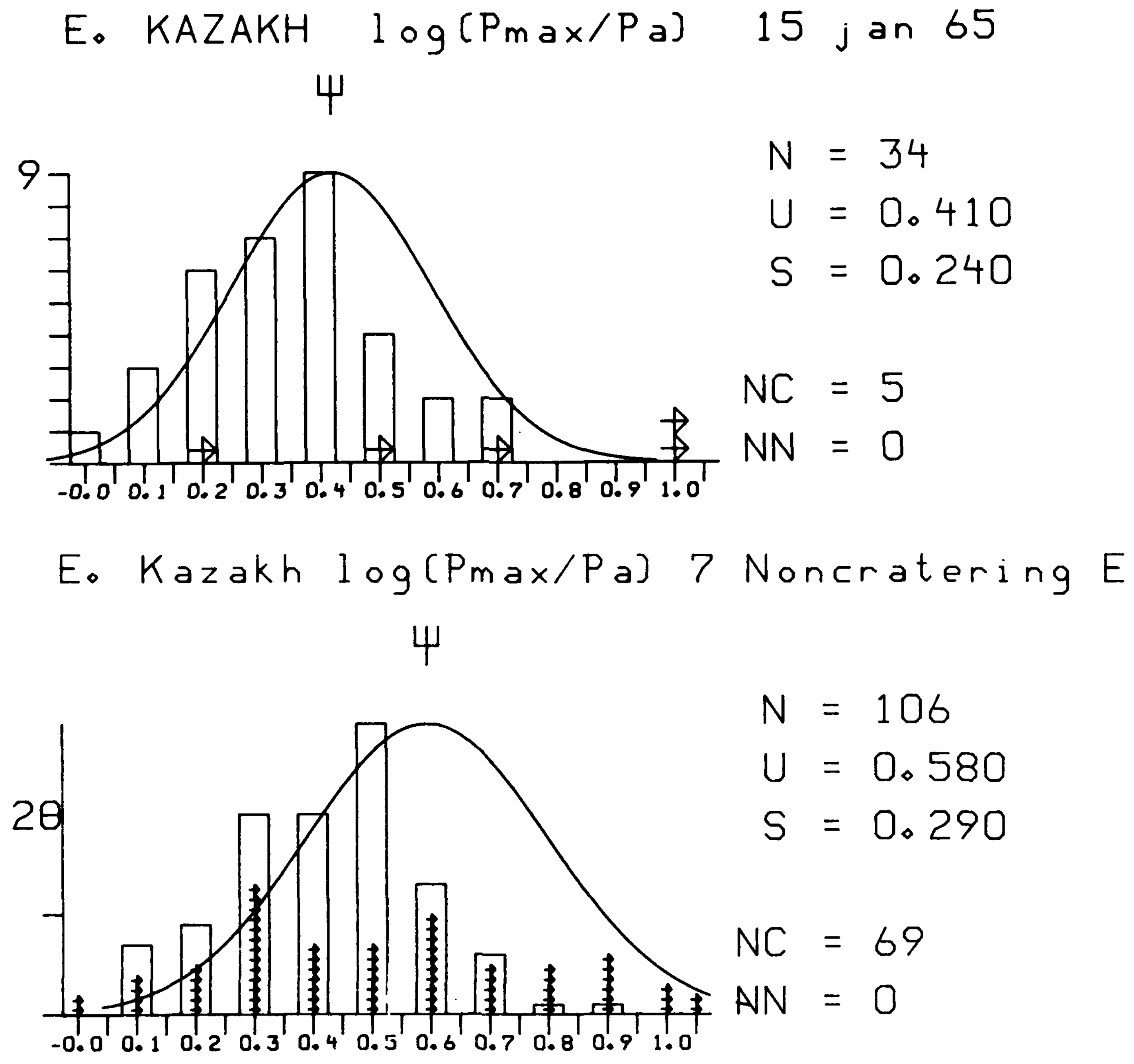
E. KAZAKH log(Pmax/Pa) 15 jan 65
Ψ
9
N = 34
U = 0.410
S = 0.240
NC = 5
NN = 0
-0.0 0.1 0.2 0.3 0.4 0.5 0.6 0.7 0.8 0.9 1.0
E. Kazakh log(Pmax/Pa) 7 Noncratering E
Ψ
20
N = 106
U = 0.580
S = 0.290
NC = 69
NN = 0
-0.0 0.1 0.2 0.3 0.4 0.5 0.6 0.7 0.8 0.9 1.0

FIGURE 7

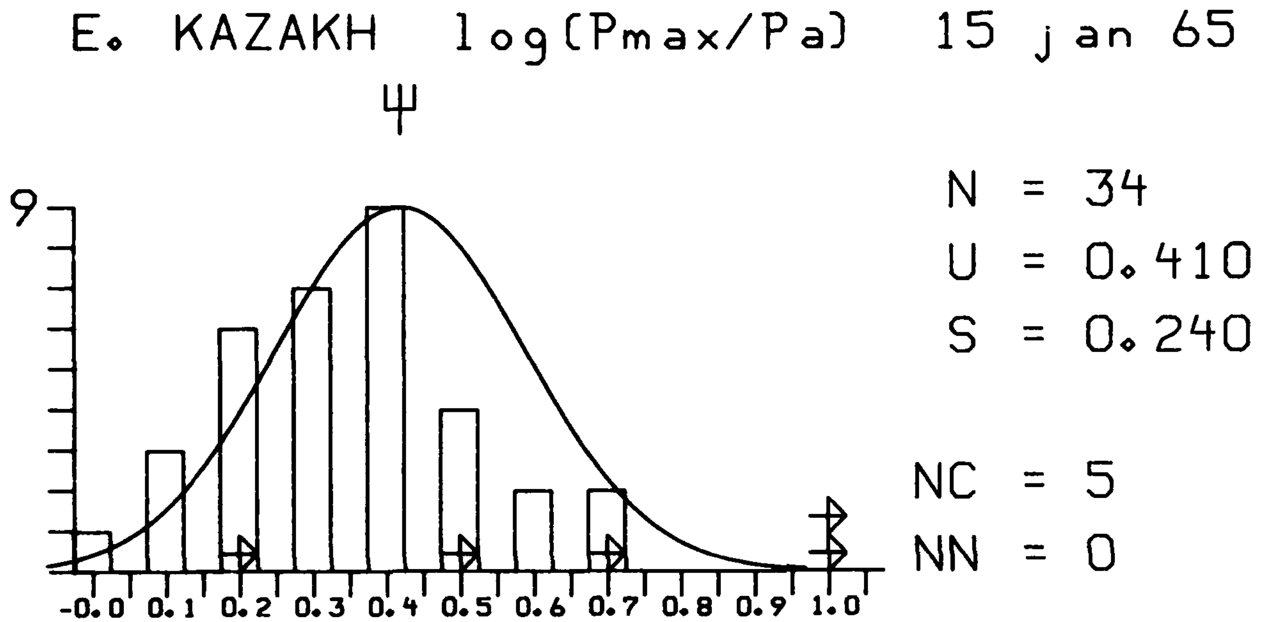
E. KAZAKH log(Pmax/Pa) 15 jan 65
ψ
9
N = 34
U = 0.410
S = 0.240
NC = 5
NN = 0
-0.0 0.1 0.2 0.3 0.4 0.5 0.6 0.7 0.8 0.9 1.0

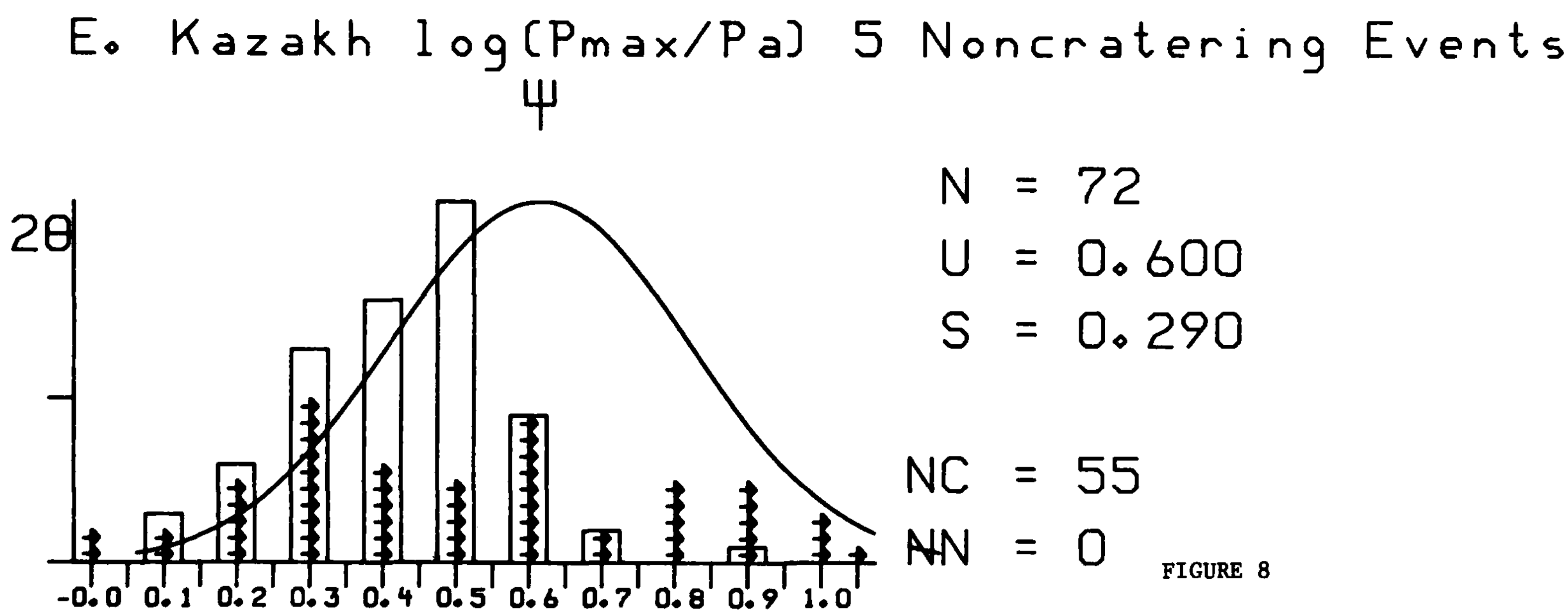
E. Kazakh log(Pmax/Pa) 5 Noncratering Events
ψ
20
N = 72
U = 0.600
S = 0.290
NC = 55
NN = 0
-0.0 0.1 0.2 0.3 0.4 0.5 0.6 0.7 0.8 0.9 1.0

FIGURE 8

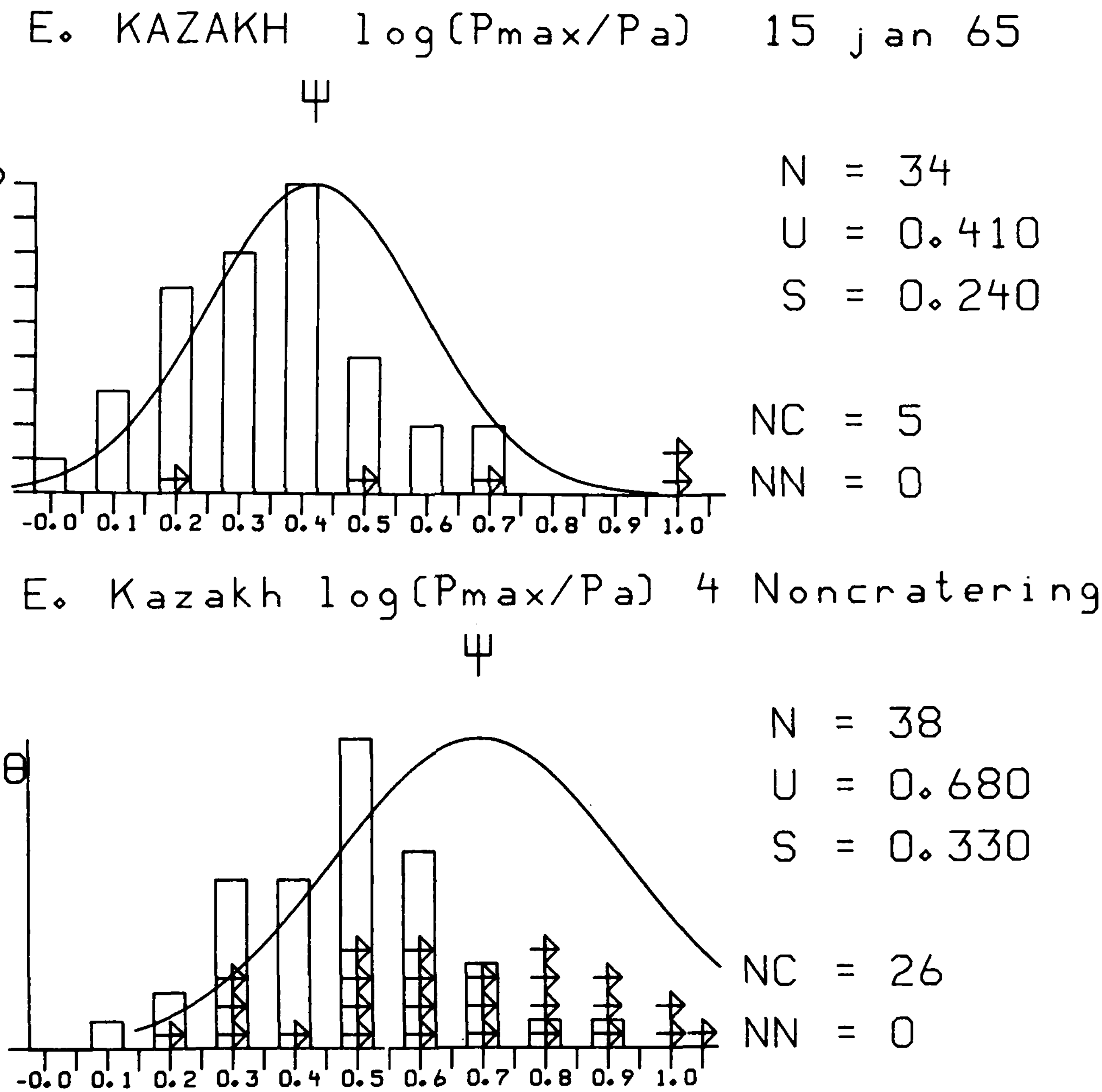
E. KAZAKH log(Pmax/Pa) 15 jan 65
Ψ
9
N = 34
U = 0.410
S = 0.240
NC = 5
NN = 0
-0.0 0.1 0.2 0.3 0.4 0.5 0.6 0.7 0.8 0.9 1.0
E. Kazakh log(Pmax/Pa) 4 Noncratering
Ψ
10
N = 38
U = 0.680
S = 0.330
NC = 26
NN = 0
-0.0 0.1 0.2 0.3 0.4 0.5 0.6 0.7 0.8 0.9 1.0

FIGURE 9

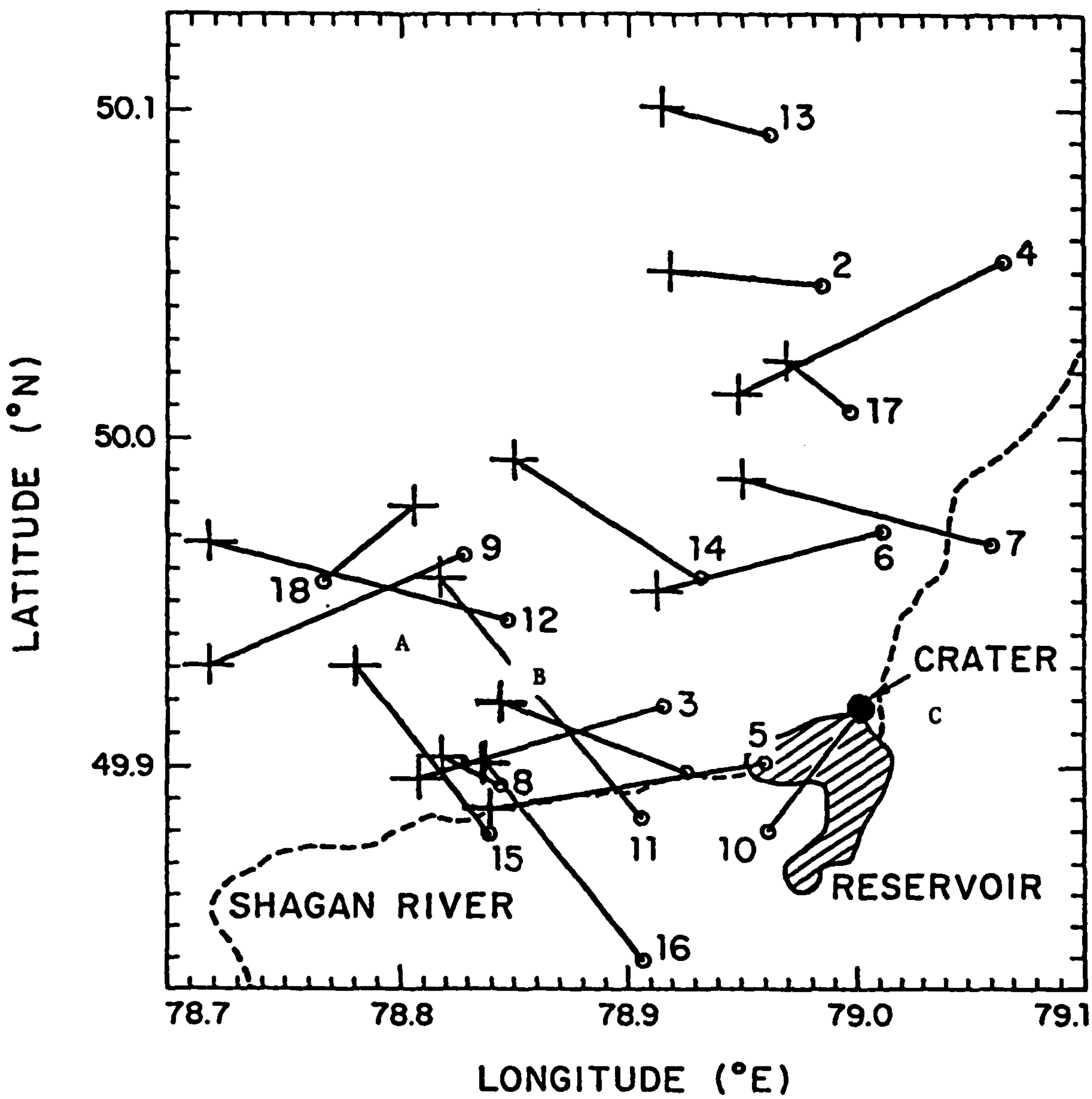

50.1
50.0
49.9
78.7
78.8
78.9
79.0
79.1
LATITUDE (°N)
LONGITUDE (°E)
13
2
4
17
7
6
14
9
18
12
A
B
CRATER
C
3
5
8
11
10
15
16
SHAGAN RIVER
RESERVOIR

FIGURE 10

DISTRIBUTION LIST
(UNCLASSIFIED REPORTS)
DARPA FUNDED PROJECTS
(Last Revised 20 Feb 1985)

RECIPIENT	NUMBER OF COPIES
DEPARTMENT OF DEFENSE	
DARPA/GSD 1400 Wilson Boulevard Arlington, VA 22209	2
DARPA/PM 1400 Wilson Boulevard Arlington, VA 22209	1
Defense Technical Information Center Cameron Station Alexandria, VA 22314	12
Defense Intelligence Agency Directorate for Scientific and Technical Intelligence Washington, D.C. 20301	1
Defense Nuclear Agency Shock Physics Directorate/SS Washington, D.C. 20305	1
Defense Nuclear Agency/SPSS ATTN: Dr. Michael Shore 6801 Telegraph Road Alexandria, VA 22310	1
DEPARTMENT OF THE AIR FORCE	
AFGL/LW ATTN: Dr. J. Cipar Terrestrial Sciences Division Hanscom AFB, MA 01730	1
AFOSR/NPG ATTN: Director Bldg 410, Room C222 Bolling AFB, Washington D.C. 20332	1
AFTAC/TG Patrick AFB, FL 32925-6471	4
AFTAC/CA (STINFO) Patrick AFB, FL 32925-6441	1
AFWL/NTESC Kirtland AFB, NM 87171	1

DEPARTMENT OF THE NAVY

NORDA 1
ATTN: Dr. J. A. Ballard
Code 543
NSTL Station, MS 39529

DEPARTMENT OF ENERGY

Department of Energy 1
ATTN: Dr. F. Dickerson (DP-52)
International Security Affairs
1000 Independence Avenue
Washington, D.C. 20545

Lawrence Livermore National Laboratory 2
ATTN: Dr. J. Hannon and Dr. M. Nordyke
University of California
P.O. Box 808
Livermore, CA 94550

Los Alamos Scientific Laboratory 1
ATTN: Dr. K. Olsen
P.O. Box 1663
Los Alamos, NM 87544

Sandia Laboratories 1
ATTN: Mr. P. Stokes
Geosciences Department 1255
Albuquerque, NM 87115

OTHER GOVERNMENT AGENCIES

Central Intelligence Agency 1
ATTN: Dr. L. Turnbull
OSI/NED, Room 5G48
Washington, D.C. 20505

U.S. Arms Control and Disarmament Agency 2
ATTN: Mrs. M. Hoinkes
Division of Multilateral Affairs
Room 5499
Washington, D.C. 20451

U.S. Geological Survey 1
ATTN: Dr. T. Hanks
National Earthquake Research Center
345 Middlefield Road
Menlo Park, CA 94025

U.S. Geological Survey 1
ATTN: Dr. Robert Masse
Global Seismology Branch
Box 25046, Stop 967
Denver Federal Center
Denver, CO 80225

UNIVERSITIES

University of California, Berkeley 1
ATTN: DR. T. McEvilly
Department of Geology and Geophysics
Berkeley, CA 94720

California Institute of Technology 1
ATTN: Dr. D. Harkrider
Seismological Laboratory
Pasadena, CA 91125

University of California, San Diego 1
ATTN: Dr. J. Orcutt
Scripps Institute of Oceanography
La Jolla, CA 92093

Columbia University 1
ATTN: Dr. L. Sykes
Lamont-Doherty Geological Observatory
Palisades, NY 10964

Massachusetts Institute of Technology 3
ATTN: Dr. S. Soloman, Dr. N. Toksoz, Dr. T. Jordan
Department of Earth and Planetary Sciences
Cambridge, MA 02139

University of Nevada, Reno 1
ATTN: Dr. A. Ryall
Seismological Laboratory
Reno, NV 89557

The Pennsylvania State University 1
ATTN: Dr. S. Alexander
Department of Mineral Sciences
University Park, PN 16802

Southern Methodist University 1
ATTN: Dr. E. Herrin
Geophysical Laboratory
Dallas, TX 75275

CIRES 1
ATTN: Dr. C. Archambeau
University of Colorado
Boulder, CO 80309

Georgia Institute of Technology 1
ATTN: Professor Anton Dainty
The School of Geophysical Sciences
Atlanta, GA 30332

St. Louis University 1
ATTN: Dr. O. Nuttli
Department of Earth and Atmospheric Sciences
3507 Laclede
St. Louis, MO 63156

DEPARTMENT OF DEFENSE CONTRACTORS

Applied Research Associates, Incorporated 1
ATTN: Dr. N. Higgins
2101 San Pedro Boulevard North East
Suite A
Albuquerque, NM 87110

Applied Theory, Incorporated 1
ATTN: Dr. J. Trulio
930 South La Brea Avenue
Suite 2
Los Angeles, CA 90036

Center for Seismic Studies 2
ATTN: Dr. Carl Romney, and Dr. William Dean
1300 N. 17th Street, Suite 1450
Arlington, VA 22209

ENSCO, Incorporated 1
ATTN: Mr. G. Young
5400 Port Royal Road
Springfield, VA 22151

ENSCO, Incorporated 1
ATTN: Dr. R. Kemerait
1930 Highway A1A
Indian Harbour Beach, FL 32937

Pacific Sierra Research Corporation 1
ATTN: Mr. F. Thomas
12340 Santa Monica Boulevard
Los Angeles, CA 90025

R&D Associates 1
ATTN: Dr. E. Martinelli
P.O. Box 9695
Marina del Rey, CA 90291

Rockwell International 1
ATTN: Dr. B. Tittmann
109 Camino Dos Rios
Thousand Oaks, CA 91360

Gould Incorporated 1
ATTN: Mr. R. J. Woodard
Chesapeake Instrument Division
6711 Baymeado Drive
Glen Burnie, MD 21061

Rondout Associates, Incorporated 1
ATTN: Dr. P. Pomeroy
P.O. Box 224
Stone Ridge, NY 12484

Science Applications, Incorporated 1
ATTN: Dr. T. Bache
P.O. Box 2351
La Jolla, CA 92038

Science Horizons
ATTN: Dr. T. Cherry and Dr. J. Minster 2
710 Encinitas Blvd
Suite 101
Encinitas, CA 92024

Sierra Geophysics, Incorporated 2
ATTN: Dr. R. Hart and Dr. G. Mellman
15446 Bell-Red Road
Redmond, WA 98052

SRI International 1
333 Ravensworth Avenue
Menlo Park, CA 94025

S-Cubed, A Division of 1
Maxwell Laboratories Inc.
Attn: Dr. Steven Day
P.O. Box 1620
La Jolla, CA 92038

S-Cubed, A Division of 1
Maxwell Laboratories Inc.
Attn: Mr. J. Murphy
11800 Sunrise Valley Drive
Suite 1212
Reston, VA 22091

Teledyne Geotech
ATTN: Dr. Z. Der & Mr. W. Rivers 2
314 Montgomery Street
Alexandria, VA 22314

Woodward-Clyde Consulants 1
ATTN: Dr. Larry Burdick
556 El Dorado St
Pasadena, CA 91105

Weidlinger Associates 1
ATTN: Dr. J. Isenberg
3000 Sand Hill Road
Menlo Park, CA 94025

NON-U.S. RECIPIENTS

National Defense Research Institute 1
ATTN: Dr. Ola Dahlman
Stockholm 80, Sweden

Blacknest Seismological Center 1
ATTN: Mr. Peter Marshall
Atomic Weapons Research Establishment
UK Ministry of Defense
Brimpton, Reading RG7-4RS
United Kingdom

NTNF NORSAR 1
ATTN: Dr. Frode Ringdal
P.O. Box 51
N-2007 Kjeller
Norway

To be determined by the project office 6